Article

Formation of Polyethylene Glycol Particles Using a Low-Temperature Supercritical Assisted Atomization Process

Hsien-Tsung Wu *, Hong-Ming Tsai and Tsung-Hsuan Li

Department of Chemical Engineering, Ming Chi University of Technology 84 Gungjuan Rd., Taishan Dist., New Taipei City 24301, Taiwan; m05138212@mail2.mcut.edu.tw (H.-M.T.); lance19950803@gmail.com (T.-H.L.)

* Correspondence: stwu@mail.mcut.edu.tw; Tel.: +886-2-2908-9899-4630; Fax: +886-2-2908-3072

Abstract: Polyethylene glycol (PEG) particles were prepared using low-temperature supercritical assisted atomization (LTSAA) with carbon dioxide as the spraying medium or the co-solute and acetone as the solvent. The effects of several key factors on the particle size were investigated. These factors included the concentration of the PEG solution, precipitator temperature, saturator temperature, ratio of the volumetric flow rate of carbon dioxide to the PEG solution, and the molecular weight of PEG. Spherical and non-aggregated PEG particles, with a mean size of 1.7–3.2 μm, were obtained in this study. The optimal conditions to produce fine particles were found to be a low concentration of the PEG solution, a low precipitator temperature, and low molecular weight of the PEG. The phase behavior of the solution mixture in the saturator presented a qualitative relationship. At the optimized volumetric flow rate ratios, the composition of CO_2 in the feed streams was near the bubble points of the saturator temperatures. X-ray and differential scanning calorimetry analyses indicated that LTSAA-treated PEG had a reduced degree of crystallinity, which could be modulated via the precipitator temperature. PEG microparticles prepared by a LTSAA process would be promising carriers for drug-controlled formulations of PEG-drug composite particles.

Keywords: low-temperature supercritical assisted atomization; polyethylene glycol

1. Introduction

Polyethylene glycol (PEG) is a hydrophilic polymer manufactured by polymerization of ethylene oxide (EO) and is commonly used in the cosmetic, food, and pharmaceutical industries. PEG exhibits outstanding biocompatibility and toxicological safety. The World Health Organization (WHO) has set the acceptable maximum daily intake of PEG in foodstuffs as 10 mg/kg body weight [1]. In pharmaceutical applications, PEG has been used as laxatives, ointments, fillings for gelatin capsules, solubilizers, tablet excipients, and carriers to improve the dissolution rate of drug. Such enhanced dissolution properties were achieved by the micronization of the drugs, transformation of the drug into a crystalline or amorphous form, the formation of a solid dispersion, and the increase of the wettability of the drug through the use of a water-soluble carrier in composite particles [2–5]. In addition, hydrophilic PEG can mask the surface of hydrophobic materials and prevent recognition by the immune system, resulting in prolonged system circulation and bypass of the RES (reticuloendothelial system) [6,7].

The conventional processes for the fabrication of PEG solids include drum flaking, jet milling, spray drying [8], and spray freezing [9]. Supercritical carbon dioxide (scCO$_2$) is a benign working medium and plays versatile roles in particle formation technologies, including RESS (rapid expansion of supercritical solutions), SAS (supercritical antisolvent), PGSS (particles from gas saturated solution), and SAA (supercritical assisted atomization). The RESS process is limited by the solubility of the

polymer in scCO$_2$ and the SAS process is not suitable for use in aqueous systems, due to the low solubility of water in scCO$_2$. The yield of the PGSS process is greater, but larger PEG particles are produced [10,11]. The SAA process can be applied in both aqueous and organic solvent systems. However, solvents with lower boiling points should be utilized in the SAA process for micronization in the low-melting point of PEG ($T_m \approx 335$ K). Adami et al. [12] proposed a new configuration of SAA, operated at reduced pressure and temperature, to micronize the thermo-sensitive compounds poly L-lactide (PLLA) and bovine serum albumin (BSA). The same group [13] used this new SAA process to produce PEG microparticles and investigated the process parameters, including the molecular weight of PEG, the precipitator temperature, the concentration of the PEG solution, and the gas to liquid ratio (GLR). The aim of the present study is to integrally investigate the influence of the low-temperature supercritical assisted atomization (LTSAA) process parameters and the phase behavior on the size and morphology of the PEG particle and the properties of the resulting PEG powder.

2. Results and Discussion

The SAA involved two atomization steps, namely, pneumatic atomization and decompressive atomization. The efficiency of decompressive atomization depends on the content of the CO$_2$ solubilized in the feed liquid solution in the saturator [14]. Therefore, the CO$_2$ content in the feed liquid can be manipulated by adjusting the flow ratio of CO$_2$ to the liquid solution, and is limited by the vapor-liquid equilibrium (VLE) phase envelopes. This hypothesis is verified by Reverchon and Antonacci [15] and our previous studies of PMMA, PMMA-co-BMA, and PMMA-co-EA particles produced via the SAA process. The composition of CO$_2$ in the feed streams at the optimized flow ratio is close to the bubble point of the saturator temperature [16–18]. Thus, phase behavior is a crucial factor in selecting the proper conditions in the SAA process. The VLE phase boundaries of carbon dioxide + acetone were obtained using the Peng–Robinson Equation with the Boston–Mathias mixing rules [19] and are presented in Figure 1. The binary interaction parameters (k_{ij} and l_{ij}) are a function of temperature and have been used to fit experimental data at different temperatures, from 303.2 K to 333.2 K in literature [20–23]. The critical properties and acentric factors for the pure components and the binary interaction parameters used are presented in Tables 1 and 2. The temperature range of the phase boundaries were included in the saturator temperature range in this study. These results could be used to qualitatively describe the relationship between the experimental conditions and the properties of the resulting PEG particles, as well as to select the appropriate conditions for the LTSAA procedure.

Table 1. Critical properties and acentric factors for pure components.

Components	T_C (K)	P_C (bar)	ω
carbon dioxide	304.1	73.8	0.239
acetone	508.1	47.0	0.304

Table 2. Interaction parameters for carbon dioxide (1) + acetone (2) system.

k_{ij}		l_{ij}	
$k_{ij}^{(1)}$	36.356	$l_{ij}^{(1)}$	20.235
$k_{ij}^{(2)}$	−0.05798	$l_{ij}^{(2)}$	−0.03273
$k_{ij}^{(3)}$	−5700.2	$l_{ij}^{(3)}$	−3131.5
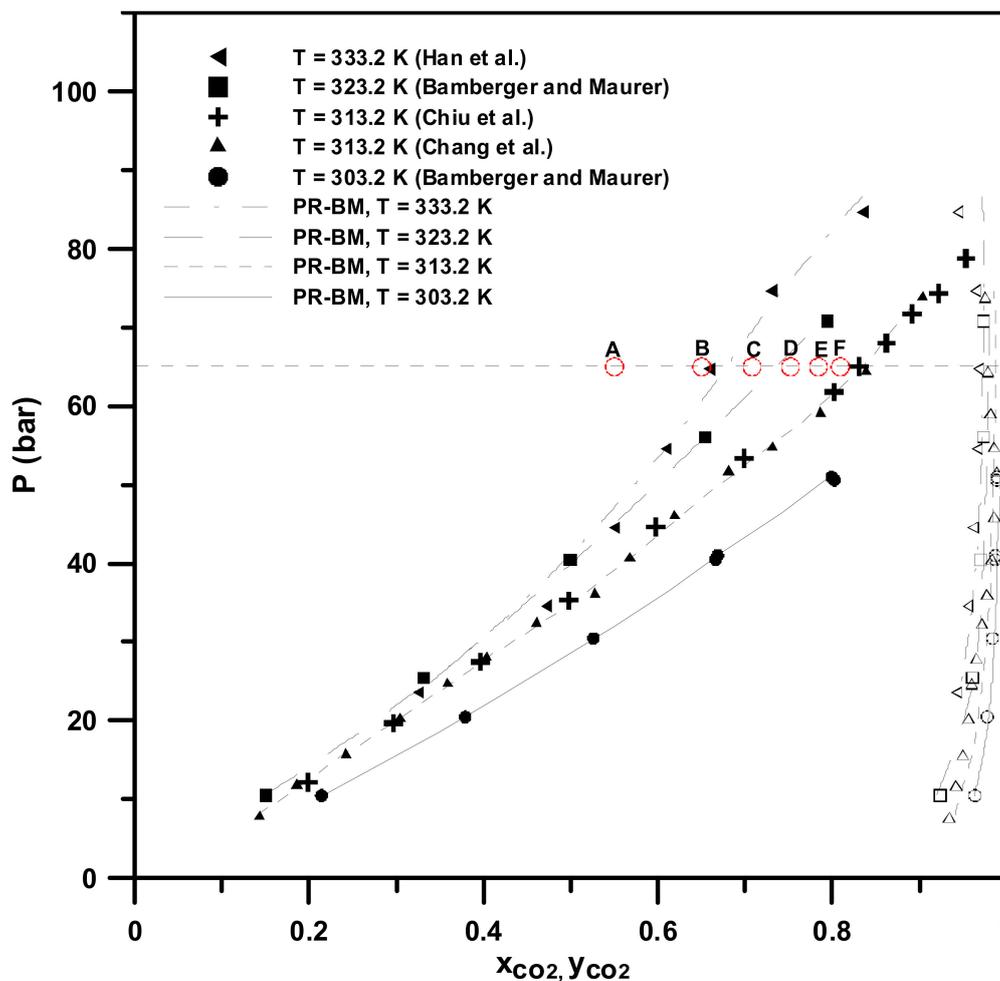
Figure 1. VLE phase diagram of the mixture of carbon dioxide + acetone. Points A, B, C, D, E, and F are referred to *R* values of 0.8, 1.2, 1.6, 2.0, 2.4, and 2.8, respectively.

Mixing rule, as follows:

$$a_M = \sum_i \sum_j x_i x_j \sqrt{a_j a_j}\left(1 - k_{ij}\right); \; k_{ij} = k_{ij}^{(1)} + k_{ij}^{(2)}T + \frac{k_{ij}^{(3)}}{T}, \tag{1}$$

$$b_M = \sum_i \sum_j x_i x_j \frac{b_i + b_j}{2}\left(1 - l_{ij}\right); \; l_{ij} = l_{ij}^{(1)} + l_{ij}^{(2)}T + \frac{l_{ij}^{(3)}}{T}. \tag{2}$$

2.1. Operation Parameters for LTSAA

The preliminary experiments were performed using conventional SAA with precipitation at atmospheric pressure [16], using a precipitation temperature of 333.2 K and a flow rate of 1.0 Nm^3/h of heated N$_2$. These experiments were unsuccessful, as a PEG film was obtained in the precipitator. This was attributed to the fact that the temperature used to evaporate the solvent during precipitation was too high for the low-melting point PEG, and thus induced particle coalescence. In subsequent experiments, the vacuum system was used to reduce the precipitator pressures and, correspondingly, lower the evaporation temperatures in the precipitator, i.e., the LTSAA process was implemented. In the preliminary LTSAA process, a precipitator pressure of 0.5 bar was achieved by the vacuum system, and a saturator temperature of 323.2 K, a solution flow rate of 3 mL/min, and a 1.0 Nm^3/h flow rate of unheated N$_2$ were used. The precipitator temperature (T_p) could be decreased to 278 K, due to

the endotherm of the evaporation heat of the solvent acetone and the Joule–Thomson effect induced by the expansion of CO_2 downstream from the nozzle. Even though the precipitator temperature (T_p) was lower than the boiling point of acetone at the precipitator pressure ($T_b = 308$ K at 0.5 bar), PEG particles were successfully produced. This might be attributed to quick drying in the highly volatile acetone and the low solubility of PEG in low-temperature acetone, even if minor acetone condensation occurred in the precipitator chamber.

The precipitation experiments were conducted at precipitator temperatures (T_p) of 273–293 K, a polymer solution concentrations (*C*) range of 10–50 mg/mL, a saturator temperature (T_s) range of 313–333 K, and volumetric flow rate ratios of carbon dioxide to the polymer solution ($R = F_{CO2}/F_l$) of 0.8–2.8. The conditions of the flow of carbon dioxide were 276 K and 6.5 MPa. This state of CO_2 was used to determine the density of CO_2 and to calculate the mole fraction composition of the feed mixture in the saturator. Table 3 lists the experimental conditions and results of the PEG particles produced by the LTSAA process. In addition, to achieve a higher precipitator temperature under the fixed saturator temperature, CO_2 flow rate, and PEG solution flow rate, the N_2 temperature was set to 473 K and 373 K (Table 3, runs #1, 2). An unheated N_2 flow was used in subsequent experiments.

Table 3. Experimental conditions and results of PEG particles.

Run	T_P	C	T_s	R	d_{no} [a]	$d_{4,3}$ [b]	PDI
	K	mg/mL	K	F_{CO2}/F_l	μm	μm	$d_{4,3}/d_{no}$
1 [c]	293	10	323	2.0	2.9 ± 0.3	3.2 ± 0.3	1.1
2 [d]	283	10	323	2.0	2.5 ± 0.2	2.9 ± 0.2	1.2
3	278	10	323	2.0	1.7 ± 0.2	2.0 ± 0.3	1.1
4	278	20	323	2.0	2.0 ± 0.3	2.3 ± 0.4	1.4
5	278	30	323	2.0	1.9 ± 0.2	2.5 ± 0.2	1.3
6	278	50	323	2.0	2.6 ± 0.2	2.9 ± 0.3	1.1
7	278	10	323	0.8	1.7 ± 0.1	2.6 ± 0.3	1.5
8	278	10	323	1.5	1.6 ± 0.2	2.2 ± 0.1	1.4
9	278	10	323	2.8	1.7 ± 0.1	2.5 ± 0.4	1.5
10	273	10	313	0.8	2.3 ± 0.2	2.9 ± 0.2	1.3
11	273	10	313	1.5	2.2 ± 0.2	2.5 ± 0.2	1.1
12	273	10	313	2.0	2.0 ± 0.3	2.2 ± 0.3	1.1
13	273	10	313	2.4	1.9 ± 0.4	2.1 ± 0.1	1.1
14	273	10	313	2.8	2.6 ± 0.4	3.0 ± 0.2	1.2
15	285	10	333	1.0	2.0 ± 0.3	2.5 ± 0.2	1.3
16	285	10	333	1.5	1.5 ± 0.2	1.7 ± 0.2	1.1
17	285	10	333	2.0	1.6 ± 0.5	2.2 ± 0.2	1.3
18	285	10	333	2.5	1.6 ± 0.5	2.3 ± 0.1	1.4
19 [e]	278	10	323	2.0	2.5 ± 0.3	2.9 ± 0.5	1.2
20 [f]	278	10	323	2.0	2.6 ± 0.3	3.2 ± 0.3	1.2

[a] $d_{no.} = \frac{\sum_{i=0}^{N} Di}{N}$, arithmetic mean size. [b] $d_{4,3} = \left(\frac{\sum_{i=0}^{N} Di^4}{\sum_{i=0}^{N} Di^3} \right)$, mass-weighted mean size. [c] $T_{N2} = 473$ K. [d] $T_{N2} = 373$ K. [e] MW = 6 kg/mole (molecular weight of PEG) [f] MW = 10 kg/mole (molecular weight of PEG).

2.2. Effects of the Precipitator Temperature and Concentration of the PEG Solution on the PEG Particle Size
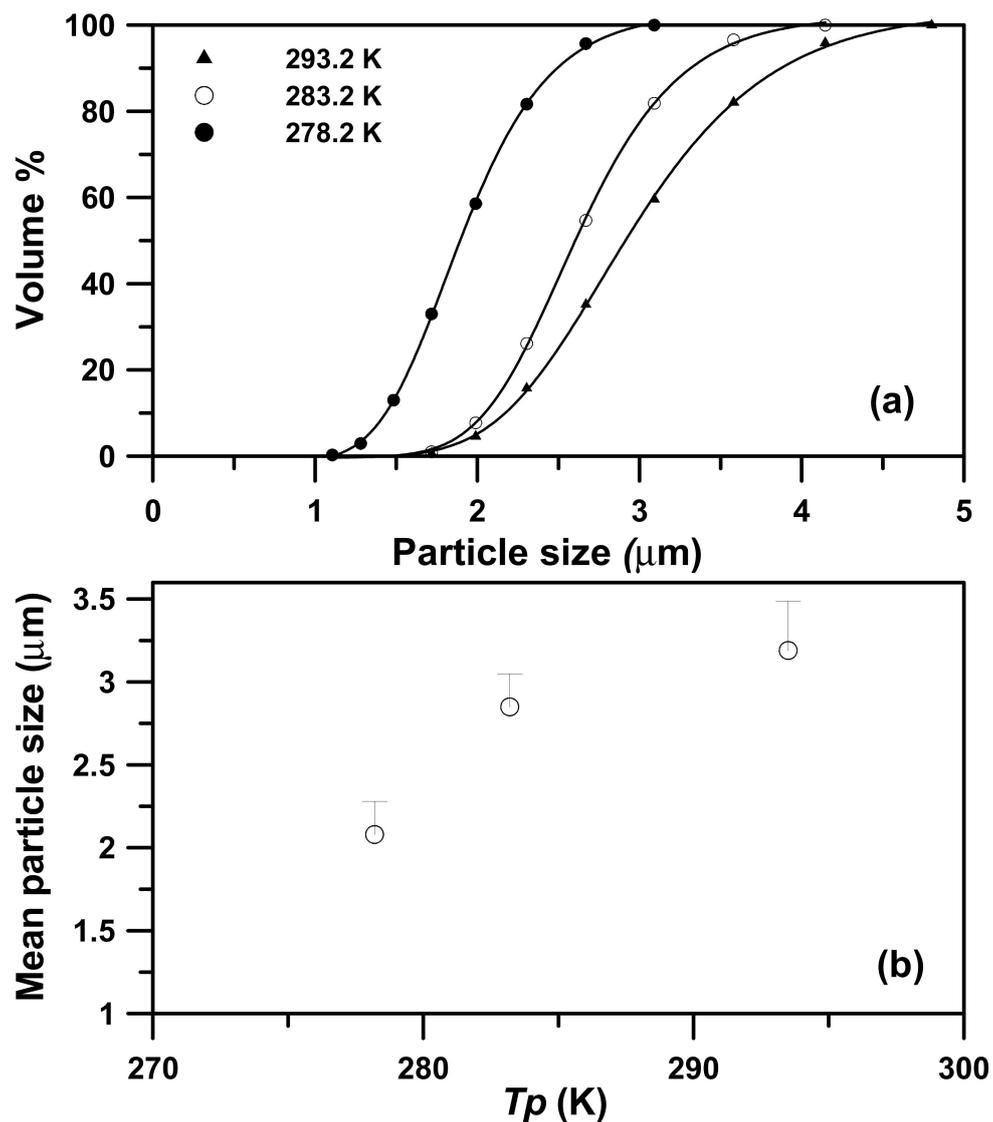
The precipitator temperature (T_p) determines whether the micronization is successful for low-melting-point PEG. This study used LTSAA and the highly volatile solvent acetone to achieve the production of PEG microparticles within the precipitator temperature range of 278 K to 293 K. The effect of the precipitator temperature on the particle sizes was examined using the following fixed conditions: A concentration (*C*) of 10 mg/mL, a saturation temperature (*Ts*) of 323.2 K, and a volume flow ratio (*R*) of 2.0 (Table 3, runs #1 to #3). Figure 2 shows the field emission scanning electron microscopy (FESEM) images of the samples with spherical micrometric particles. The particle sizes distribution (PSD) (Figure 3a) and mean size of PEG particles (Figure 3b) increased with the precipitator temperature. Although a high temperature is conducive to rapid evaporation, it will cause the particles

to soften and aggregate into larger particles. Similar results have been reported for other relevant SAA processes [13,24].

The effect of the concentration of the PEG solution on the particle sizes was examined in the concentration (C) range of 10–50 mg/mL, at a saturator temperature (T_S) of 323.2 K, and a volume flow ratio (R) of 2.0 (Table 3, runs #3 to #6). Figure 4 shows the FESEM images of the samples with spherical micrometric particles. The PSD (Figure 5a) and mean size of the PEG particles (Figure 5b) increased with the concentration of the PEG solution, thus indicating that the high viscosity of the high concentration PEG solution resulted in larger liquid droplets and increased PEG particle sizes. Similar results have been reported, mostly for relevant SAA processes [13–18,25–32].
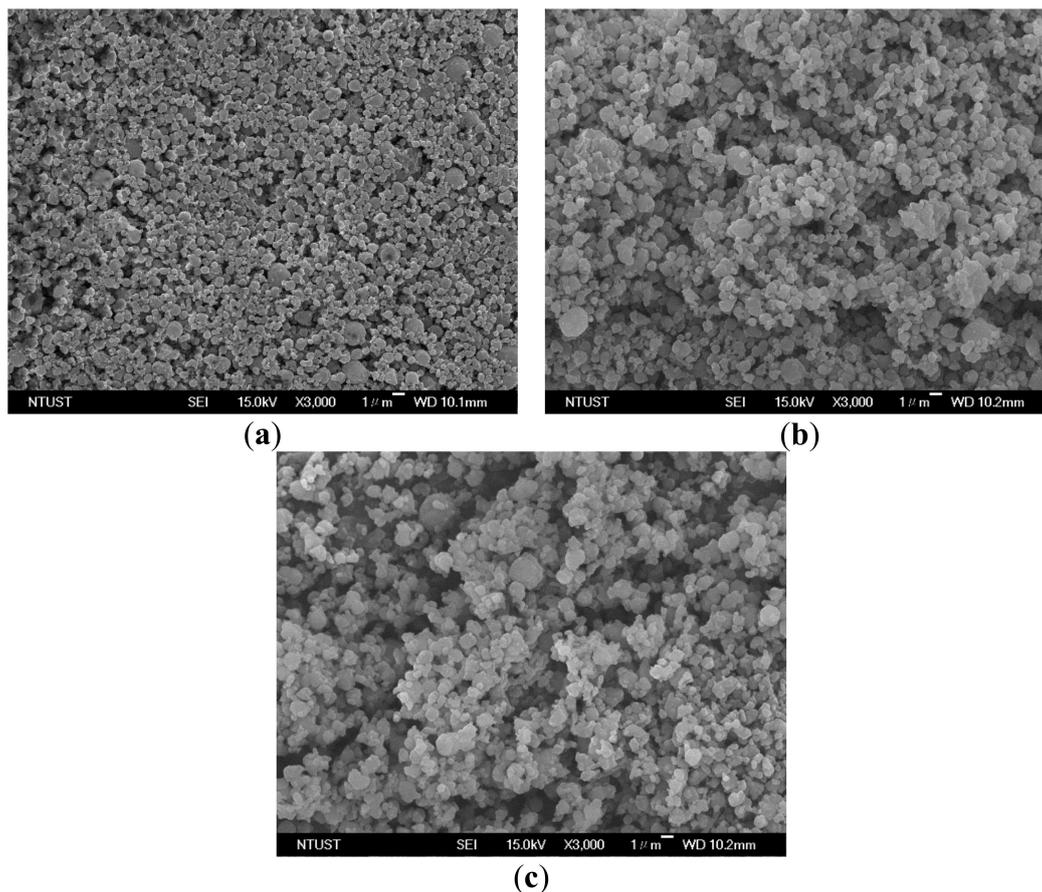

Figure 2. FESEM images of PEG particles produced by LTSAA process at different precipitator temperatures (T_P): (**a**) T_P = 278.2 K. (**b**) T_P = 283.2 K. (**c**) T_P = 293.2 K.

Figure 3. (**a**) The particle size distributions of the sample produced by the LTSAA process at different precipitator temperatures (T_P), from 278.2 K to 293.2 K. (**b**) Mass-weighted mean particle size ($\bigcirc$) varying with precipitator temperature (T_P) at C = 10 mg/mL, T_S = 323.2 K, R = 2, and MW = 4000.
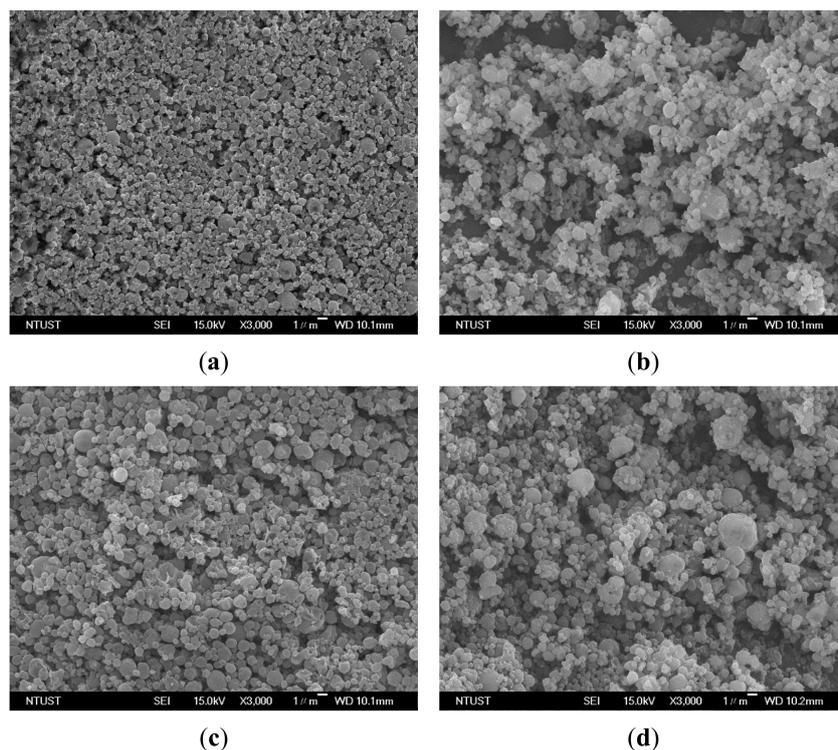
Figure 4. FESEM images of PEG particles produced by the LTSAA process at different concentrations of the PEG solution (*C*): (**a**) *C* = 10 mg/mL; (**b**) *C* = 20 mg/mL; (**c**) *C* = 30 mg/mL; (**d**) *C* = 50 mg/mL.
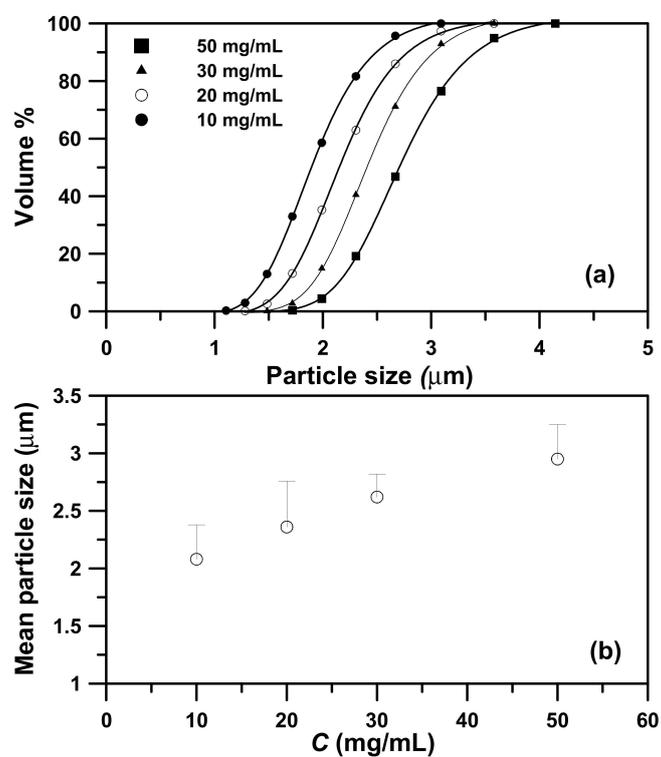

Figure 5. The particle size distributions of the sample produced by the LTSAA process at different concentrations of the PEG solution (*C*) from 10 mg/mL to 50 mg/mL. (**b**) Mass-weighted mean particle size (○) varying with the concentration of the PEG solution (*C*) at T_S = 323.2 K, *R* = 2, and *MW* = 4000.

2.3. Effects of the Phase Behavior and Molecular Weight of PEG on the PEG Particle Size

As described in Section 2, the composition of CO_2 in the feed liquid can be manipulated by altering the flow ratio of CO_2 to the liquid solution in the standard SAA process, and is limited by the VLE phase envelopes. However, the effect of phase behavior on the PEG particle size in the LTSAA process has not yet been investigated. The mean sizes of the PEG particles produced at different flow ratios (R) and saturator temperatures (T_S) are presented in Table 3 (runs #3, #7 to #18). Figure 6 presents the FESEM images of samples with different flow ratios. Increasing R values favored smaller particles, but the optimal R value of 2.0 (Figure 6c) occurred at a saturator temperature of 323 K. The same results are also observed in Figure 7. The different saturator temperatures exhibited the following optimal R values: $R = 1.5$ at $T_S = 333.2$ K; $R = 2.0$ at $T_S = 323.2$ K; and $R = 2.4$ at $T_S = 313.2$ K.

Based on the VLE phase boundaries for different temperatures (Figure 1), the composition of CO_2 in the saturated compressed-liquids (bubble point) was approximately $R = 1.2$–1.6 (333.2 K), $R = 2.0$ (333.2 K), and $R = $ ~2.8 (313.2 K), respectively. These results were consistent with the optimized R values shown in Figure 7 at 333.2 K and 323.2 K. When the flow ratios were further increased, the operating conditions fell into the vapor-liquid coexistence region. The concentration of the PEG solution may have risen by acetone, soluble in CO_2-rich vapor, producing the larger particles. The optimal R value was slightly less than that of the 313.2 K bubble point at $R = 2.8$, which was attributed to the anti-solvent effect induced by the fact that the mole fraction of CO_2 in the saturated compressed-liquids was greater than 0.80. Based on these results and on previous studies of polymer micronization via the SAA process using acetone as the solvent [15–18], the importance of phase behavior in the LTSAA process was once again verified.
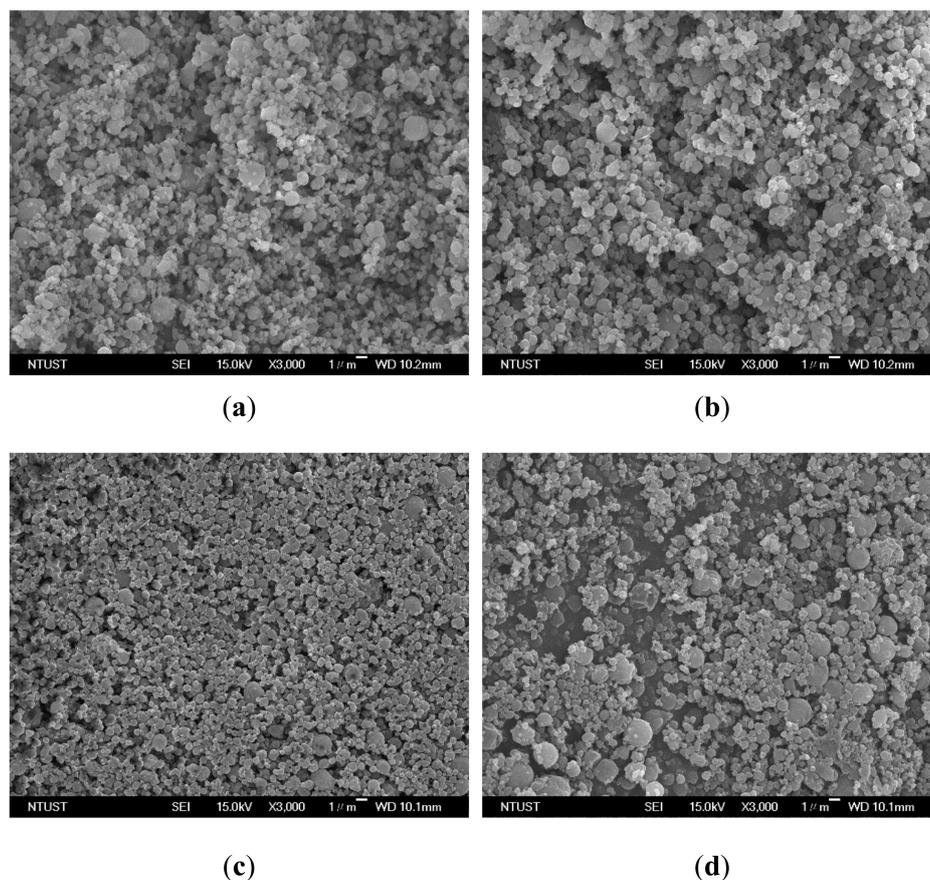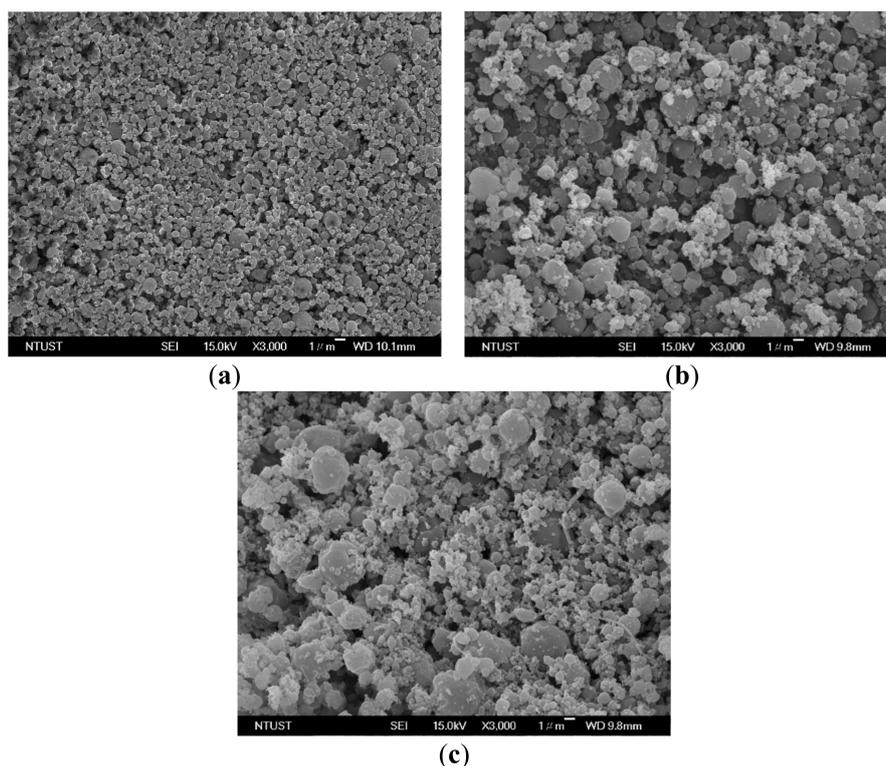

Figure 6. FESEM images of PEG particles produced by the LTSAA process at different volume flow ratios (R): (**a**) $R = 0.8$; (**b**) $R = 1.5$; (**c**) $R = 2$; and (**d**) $R = 2.8$.
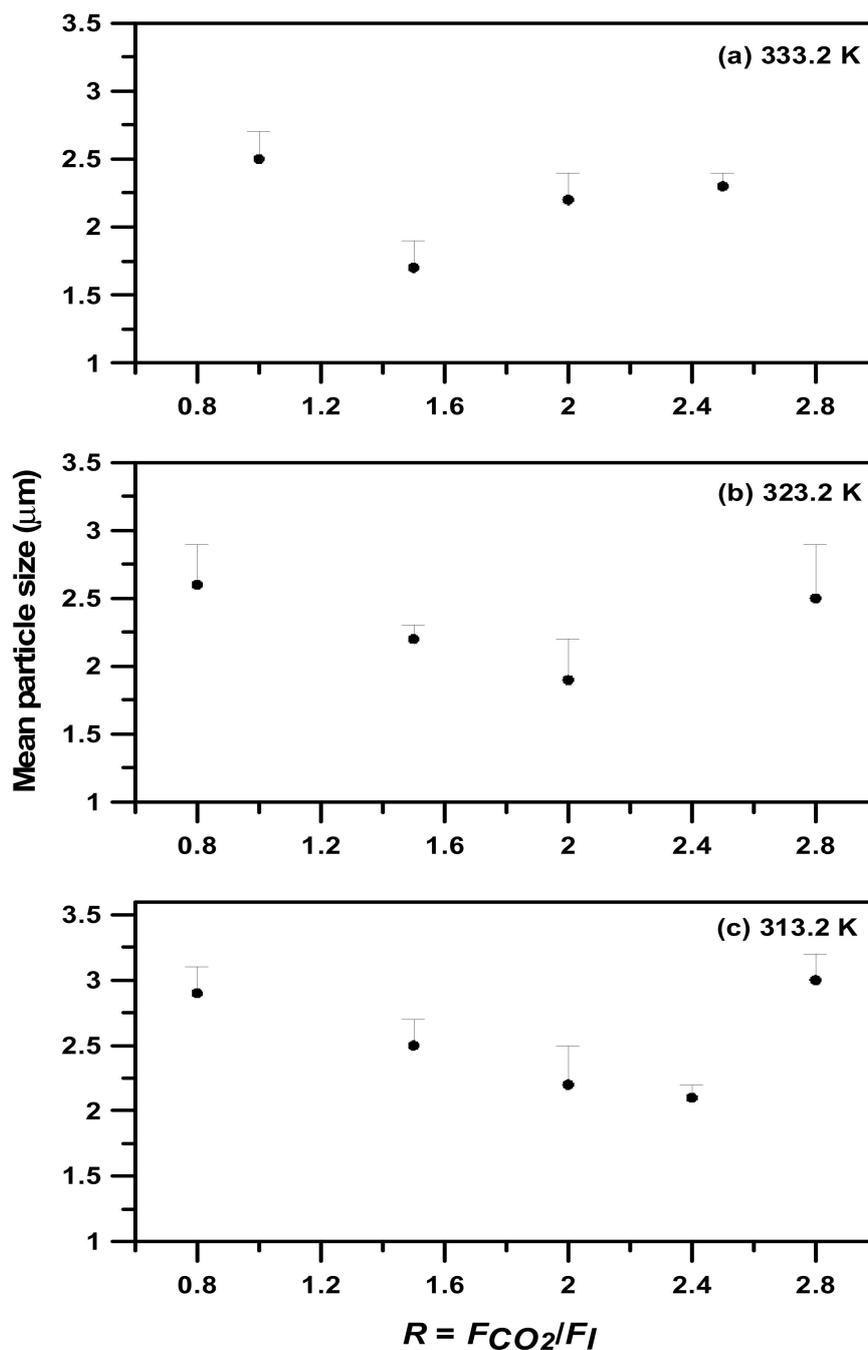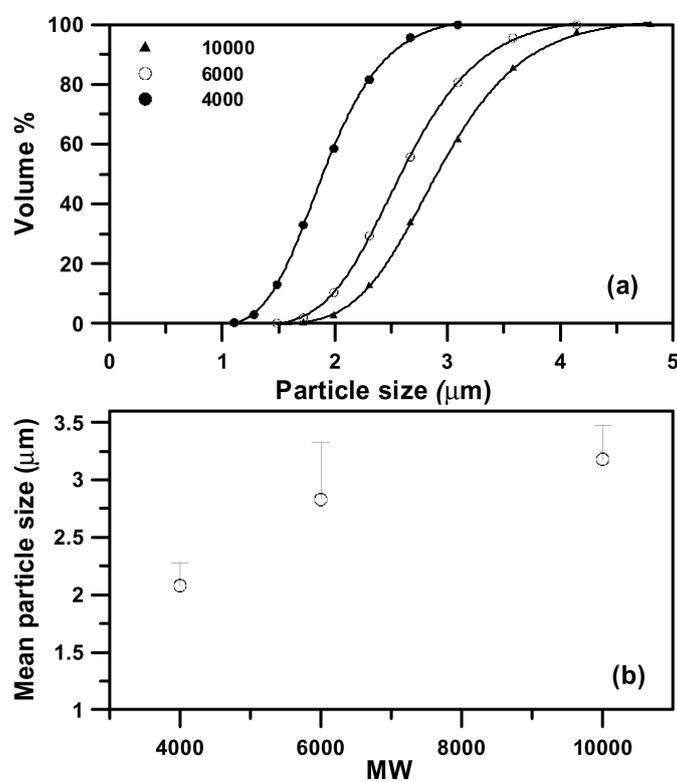
Figure 7. Mass-weighted mean particle size (●) varying with volume flow ratio (*R*) at *C* = 10 mg/mL and saturator temperatures: (**a**) T_S = 333.2 K, (**b**) T_S = 323.2 K, (**c**) T_S = 313.2 K.

The effect of the molecular weight (MW) of PEG on the particle size was also investigated in runs #3, #19 and #20. Figures 8 and 9 present the FESEM images and PSD of samples with different MW. The mean sizes of PEG particles increase with the MW of PEG. This was attributed to the higher viscosity of a higher MW in the PEG solution. The same results were also presented in Liparoti et al. [13].

Figure 8. FESEM images of PEG particles produced by the LTSAA process at different molecular weights of PEG (*MW*): (**a**) *MW* = 4000, (**b**) *MW* = 6000, (**c**) *MW* = 10,000.

Figure 9. (**a**) The particle size distributions of the sample produced by the LTSAA process at different molecular weights of PEG (*MW*) from 4000 to 10000. (**b**) Mass-weighted mean particle size (○) varying with molecular weight of PEG (*MW*) at C = 10 mg/mL, T_S = 323.2 K, and R = 2.

2.4. Solid Characterization

Figures 10 and 11 show the X-ray diffraction (XRD) and differential scanning calorimetry (DSC) analyses of the as-received and LTSAA-processed PEG particles, respectively. The XRD results showed a reduction in the intensity of the characteristic peaks (19.2°, 23.4°) of all the LTSAA-PEG particles, compared to those of the as-receive PEG, which in turn suggested the presence of amorphous polymer and/or metastable folded forms in the LTSAA-PEG powder samples. Similar decreased crystallinity has been observed, mainly in SAA-related polymer particles, e.g., PMMA, PLLA, chitosan, and IMC-CH composite [3,12,15,31]. However, the presence of crystalline particles produced by the SAA process was still observed in some materials, e.g., mannitol and PEG, and was attributed to the crystallization rate being higher than the evaporation rate [13,32]. This hypothesis was demonstrated by the PEG particles prepared at different precipitator temperatures (Figure 10b–d). The magnitude of the XRD peak, 23.4°, was further reduced as the precipitator temperature was increased (23% to 42%). Based on the DSC analyses (Figure 11), the fusion heat of the raw PEG-4000 was 178.6 ± 0.5 J/g, while those of the LTSAA samples treated at precipitator temperatures of 278.2 K, 283.2 K, and 293.2 K (Figure 11d–b) decreased to 177.0 ± 0.4, 170.0 ± 0.6, and 155.0 ± 0.3 J/g, respectively. The LTSAA-treated samples with lower fusion heats exhibited reduced crystallinity at higher precipitator temperatures.

For the LTSAA-treated samples of higher MW PEG particles (PEG6000 and PEG10000), the magnitude of the XRD peak at 23.4° reduced by 38% and 30%, respectively. A higher reduction in the magnitude of the XRD peak corresponded to higher reduction in the fusion heat of LTSAA-PEG6000 (141.2 ± 1.2 J/g), as compared with that of raw PEG6000 (182.2 ± 0.6 J/g). High MW PEG10000 exhibited lesser reduction in the magnitude of the XRD peak—the fusion heat of LTSAA-PEG10000 was 174.8 ± 0.7 J/g, while that of raw PEG10000 was 178.2 ± 0.7 J/g. This could be attributed to the lower segmental mobility and more convenient geometrical alignment of high MW PEG [33]. The decrease in that magnitude of the XRD peaks and the fusion heats confirmed the reduction in the crystallinity of the LTSAA-treated PEG particles. Similar results were also presented for PEG particles prepared by spray drying from 95% ethanol [34]. Additionally, DSC analyses demonstrated that the melting points of PEG decreased with the molecular weight of PEG [35,36], and that the precipitator temperature and PEG particle size had a minor impact on the melting points of PEG.
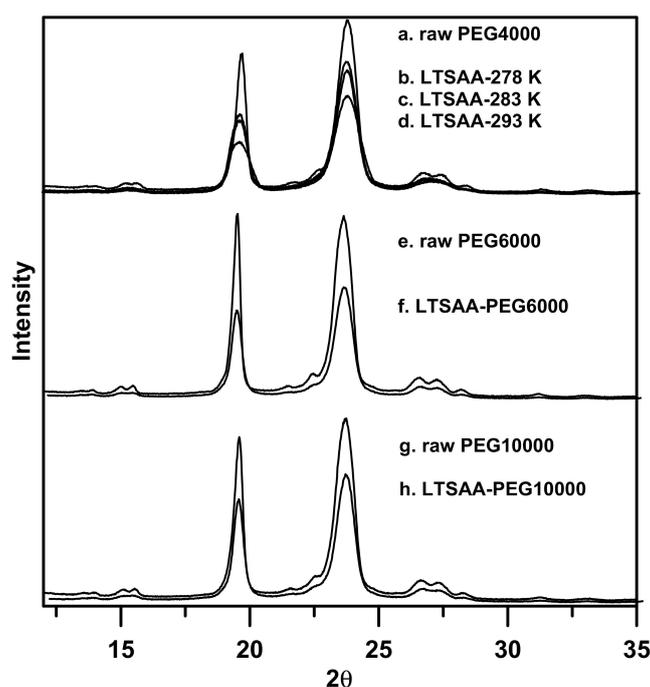

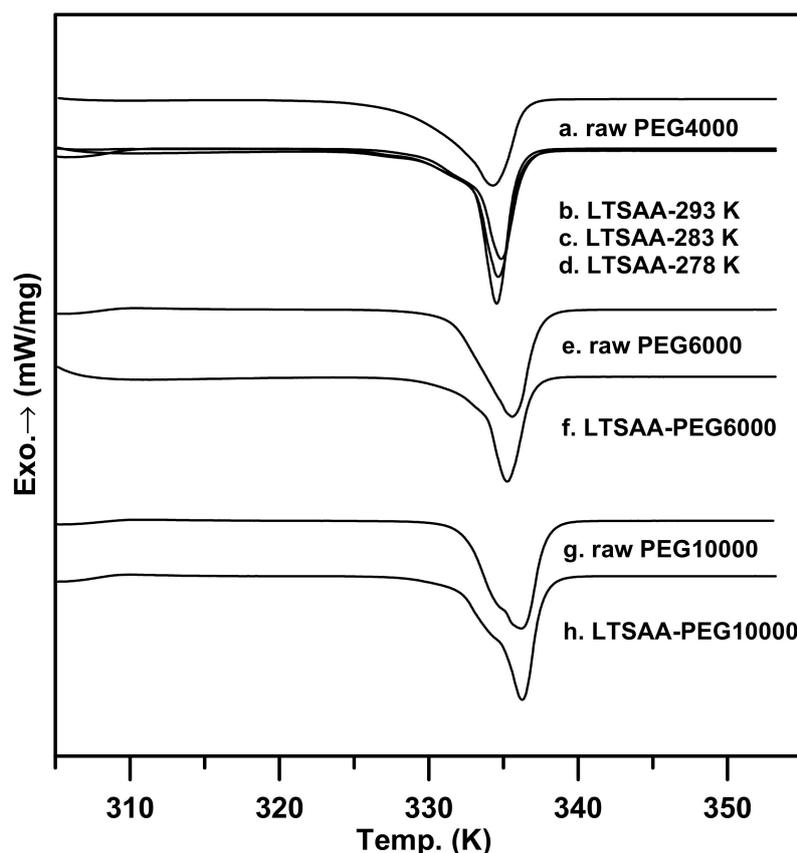**Figure 10.** The XRD analyses of the PEG particles produced using LTSAA.

Figure 11. The DSC analyses of the PEG particles produced using LTSAA.

## 3. Materials and Methods

3.1. Materials

Poly ethylene glycol (PEG, average MW = 4, 6, and 10 kg/mol) was purchased from Aldrich, USA. Acetone (99.9% purity, HPLC grade) was purchased from Tedia, USA. Carbon dioxide (99.9% purity) and nitrogen (99.9% purity) were purchased from Yung-Ping Gas Co., Taiwan. These chemicals were used without further purification.

3.2. Production of PEG Particles

Figure 12 shows a schematic diagram of the LTSAA apparatus installed in the present study. The apparatus consisted of a saturator (8), precipitator (10), cold trap (14), and three feeding lines. A high-pressure vessel (Model: 7973, 24 cm^3, Applied Separations, Allentown, PA, USA) served as the saturator and was loaded with protruding stainless-steel packing that provides a large contact area between the PEG solution and the CO_2. The solution in the saturator was sprayed through the nozzle (9) (internal diameter, 130 μm) into the precipitator. The saturator was located in a thermostatic circulating water bath (5), which was regulated to within ± 0.1 K. A metal frit (11) mounted at the bottom of the precipitator outlet retains the PEG particles. Downstream from the precipitator, a cold trap (14) (CT10/−50 °C, Firstek, Taipei, Taiwan) and vacuum pump (15) (G-100D, ULVAC, Chigasaki, Kanagawa, Japan) were used to recover the solvent and gas at reduced pressure. The three feeding lines contained the PEG solution (4), CO_2, and N_2. Two high-pressure liquid pumps were used to deliver CO_2 (2) (NP-KX-540, Nihon Seimitsu Kagaku Co., Hon-cho, Kawaguchi, Japan) and the PEG solution (3) (PU-1580, JASCO, Hachioji, Tokyo, Japan). The N_2 flow from the cylinder was controlled by a mass controller (6) (251-FKASBYAA, Porter, Hatfield, PA, USA) and heated in an electric heat

exchanger (7) (series 93, Watlow, St. Louis, MO, USA), and was sent to the precipitator to facilitate the evaporation of the liquid droplets.

The experimental procedure is described here briefly. The CO_2 flow rate (F_{CO2}) and saturator temperature (T_S) were preset. The saturator pressure was set at 6.5 ± 0.2 MPa. After a steady state was achieved, the PEG solution was introduced into the saturator at a flow rate of 3 mL/min. The PEG solution containing the dissolved CO_2 was sprayed through the injection nozzle to atomize the liquid as it entered the precipitator. When the atomized solution came into contact with the heated N_2 (1.0 Nm^3/h), the solvent evaporated from the droplets, resulting in the supersaturation of the PEG particles. Samples of the product were collected from the precipitator and observed using FESEM (model 6500, JEOL, Akishima, Tokyo, Japan).
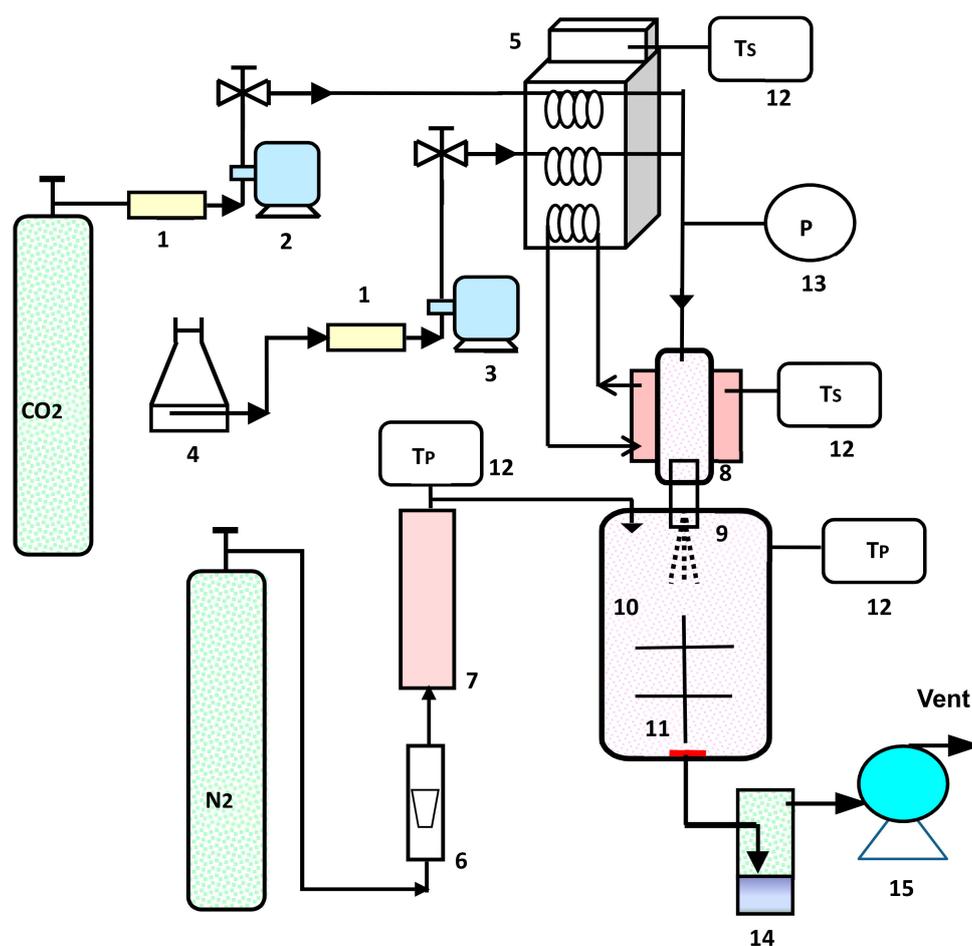
1 Filter	6 Mass controller	11 Metal frit
2 Liquid pump	7 Heat exchanger	12 Thermometer
3 HPLC pump	8 Saturator	13 Pressure gauge
4 PEG solution	9 Nozzle	14 Cold trap
5 Water bath	10 Precipitator	15 Vacuum pump

Figure 12. Apparatus of low-temperature supercritical assisted atomization (LTSAA).

The PSD and the mean size (the arithmetic mean particle sizes, d_{no}, and the mass-weighted mean sizes, $d_{4,3}$) of the PEG particle were determined using a dynamic light scattering (DLS) particle analyzer (Zatasizer Nano ZS90, Malvern, UK). Before analysis, the PEG particles were suspended in 278 K acetone and sonicated for 1 min. All precipitation experiments were performed in triplicate at minimum and used to calculate the mean values, with standard deviation, for each set of conditions.

The average yield of the PEG particles using LTSAA was 80%. The weight loss was attributed to the adherence of some fraction of the PEG microparticles to the walls of the precipitator and inside the pores of the filter.

3.3. Solid-State Characterization

The X-ray diffraction (XRD) patterns of the powder products were recorded using an X'Pert Pro X-ray powder diffractometer (PANalytical, Almelo, Netherlands). The scanning region of the diffraction angle (2θ) ranged from 10° to 50° at a scan rate of 0.02°/s. Thermograms of the PEG samples were obtained using low a temperature differential scanning calorimeter (LT-DSC, Netzsch 204 Fl Phoenix, Wittelsbacherstraße, Selb, Germany). Samples of 3–5 mg were placed in aluminum pans and the pans were sealed and heated from 298.2 K to 353.2 K at a rate of 5 K/min in N_2 atmosphere.

4. Conclusions

In this study, spherical and non-aggregated PEG particles were prepared using the LTSAA process, with CO_2 as the spraying medium or the co-solute and acetone as the solvent. The experimental results showed that the mean size of the PEG particles decreased with the concentration of the PEG solution, precipitator temperature, and molecular weight of PEG. At the optimized volumetric flow rate ratios, the composition of CO_2 in the feed streams was near the bubble points of the saturator temperatures. X-ray and DSC analyses indicated that LTSAA-treated PEG had a reduced degree of crystallinity, which could be decreased further by increasing the precipitator temperature. The different morphologies of PEG microparticles prepared by the LTSAA process would be promising carriers, and investigation of the dissolution rate of drug-controlled formulations of PEG-drug composite particles is in progress.

Author Contributions: All authors contributed to this study. Conceptualization, H.-T.W.; methodology, H.-T.W.; investigation, H.-M.T. and T.-H.L.; formal analysis, H.-M.T. and T.-H.L.; writing, H.-T.W. All the authors approved the final version of the paper.

Conflicts of Interest: The authors declare no conflict of interest.

References

1. Committee on Food Additives. Evaluation of certain food additives. Twenty-third Report of the Joint FAO/WHO Expert. *TRS 931* **1980**, *648*, 17–18.
2. Noyes, A.A.; Whitney, W.R. The rate of solution of solid substances in their own solutions. *J. Am. Chem. Soc.* **1897**, *19*, 930–934. [CrossRef]
3. Wu, H.-T.; Yang, C.-P.; Huang, S.-C. Dissolution enhancement of indomethacin-chitosan hydrochloride composite particles produced using supercritical assisted atomization. *J. Taiwan Inst. Chem. Eng.* **2016**, *67*, 98–105. [CrossRef]
4. Dos Santos, K.M.; Barbosa, R.M.; Vargas, F.G.A.; de Azevedo, E.P.; Lins, A.C.D.S.; Camara, C.A.; Aragão, C.F.S.; Moura, T.F.L.E.; Raffin, F.N. Development of solid dispersions of β-lapachone in PEG and PVP by solvent evaporation method. *Drug Dev. Ind. Pharm.* **2018**, *44*, 750–756. [CrossRef] [PubMed]
5. Ahuja, N.; Katare, O.P.; Singh, B. Studies on dissolution enhancement and mathematical modeling of drug release of a poorly water-soluble drug using water-soluble carriers. *Eur. J. Pharm. Biopharm.* **2007**, *65*, 26–38. [CrossRef] [PubMed]
6. Craig, D.Q.M. A review of thermal methods used for the analysis of the crystal form, solution thermodynamics and glass transition behaviour of polyethylene glycols. *Thermochim. Acta* **1995**, *248*, 189–203. [CrossRef]
7. Owens III, D.E.; Peppas, N.A. Opsonization, biodistribution, and pharmacokinetics of polymeric nanoparticles. *Int. J. Pharm.* **2006**, *307*, 93–102. [CrossRef] [PubMed]

8. Weuts, I.; Kempen, D.; Verreck, G.; Decorte, A.; Heymans, K.; Peeters, J.; Brewster, M.; Van den Mooter, G. Study of the physicochemical properties and stability of solid dispersions of loperamide and PEG6000 prepared by spray drying. *Eur. J. Pharm. Biopharm.* **2005**, *59*, 119–126. [CrossRef] [PubMed]

9. Barron, M.K.; Young, T.J.; Johnston, K.P.; Williams 3rd, R.O. Investigation of processing parameters of spray freezing into liquid to prepare polyethylene glycol polymeric particles for drug delivery. *AAPS PharmSciTech* **2003**, *4*, E12. [CrossRef]

10. Hao, J.; Whitaker, M.J.; Serhatkulu, G.; Shakesheff, K.M.; Howdle, S.M. Supercritical fluid assisted melting of poly(ethylene glycol): A new solvent-free route to microparticles. *J. Mater. Chem.* **2005**, *15*, 1148–1153. [CrossRef]

11. Nalawade, S.P.; Picchioni, F.; Janssen, L.P.B.M. Batch production of micron size particles from poly(ethylene glycol) using supercritical CO2 as a processing solvent. *Chem. Eng. Sci.* **2007**, *62*, 1712–1720. [CrossRef]

12. Adami, R.; Liparoti, S.; Reverchon, E. A new supercritical assisted atomization configuration, for the micronization of thermolabile compounds. *Chem. Eng. J.* **2011**, *173*, 55–61. [CrossRef]

13. Liparoti, S.; Adami, R.; Reverchon, E. PEG micronization by supercritical assisted atomization, operated under reduced pressure. *J. Supercrit. Fluids* **2012**, *72*, 46–51. [CrossRef]

14. Reverchon, E. Supercritical-assisted atomization to produce micro- and/or nanoparticles of controlled size and distribution. *Ind. Eng. Chem. Res.* **2002**, *41*, 2405–2411. [CrossRef]

15. Reverchon, E.; Antonacci, A. Polymer microparticles production by supercritical assisted atomization. *J. Supercrit. Fluids* **2007**, *39*, 444–452. [CrossRef]

16. Wu, H.-T.; Yang, M.-W. Precipitation kinetics of PMMA sub-micrometric particles with a supercritical assisted-atomization process. *J. Supercrit. Fluids* **2011**, *59*, 98–107. [CrossRef]

17. Wu, H.-T.; Yang, M.-W. Precipitation kinetics of PMMA-co-BMA sub-micrometric particles with compressed CO2 assisted-atomization process. *Powder Technol.* **2012**, *228*, 91–99. [CrossRef]

18. Wu, H.-T.; Yang, M.-W.; Huang, S.-C. Sub-micrometric polymer particles formation by a supercritical assisted-atomization process. *J. Taiwan Inst. Chem. Eng.* **2014**, *45*, 1992–2001. [CrossRef]

19. Mathias, P.M.; Klotz, H.C.; Prausnitz, J.M. Equation-of-State mixing rules for multicomponent mixtures: The problem of invariance. *Fluid Phase Equilibria* **1991**, *67*, 31–44. [CrossRef]

20. Han, F.; Xue, Y.; Tian, Y.; Zhao, X.; Chen, L. Vapor–liquid equilibria of the carbon-dioxide + acetone system at pressures from (2.36 to 11.77) MPa and temperatures from (333.15 to 393.15) K. *J. Chem. Eng. Data* **2005**, *50*, 36–39. [CrossRef]

21. Bamberger, A.; Maurer, G. High-pressure (vapour + liquid) equilibria in (carbon dioxide + acetone or 2-propanol) at temperatures from 293 K to 333 K. *J. Chem. Thermodyn.* **2000**, *32*, 685–700. [CrossRef]

22. Chiu, H.-Y.; Lee, M.-J.; Lin, H.-M. Vapor−liquid phase boundaries of binary mixtures of carbon dioxide with ethanol and acetone. *J. Chem. Eng. Data* **2008**, *53*, 2393–2402. [CrossRef]

23. Chang, C.J.; Day, C.-Y.; Ko, C.-M.; Chiu, K.-L. Densities and P-x-y diagrams for carbon dioxide dissolution in methanol, ethanol, and acetone mixtures. *Fluid Phase Equilibria* **1997**, *131*, 243–258. [CrossRef]

24. Reverchon, E.; Adami, R.; Scognamiglio, M.; Fortunato, G.; Della Porta, G. Beclomethasone microparticles for wet Inhalation, produced by supercritical assisted atomization. *Ind. Eng. Chem. Res.* **2010**, *49*, 12747–12755. [CrossRef]

25. Cai, M.-Q.; Guan, Y.-X.; Yao, S.-J.; Zhu, Z.-Q. Supercritical fluid assisted atomization introduced by hydrodynamic cavitation mixer (SAA-HCM) for micronization of levofloxacin hydrochloride. *J. Supercrit. Fluids* **2008**, *43*, 524–534. [CrossRef]

26. Liparoti, S.; Adami, R.; Reverchon, E. Supercritical Assisted Atomization: effect of operative conditions on PVP microparticle size and morphology. *J. Supercrit. Fluids* **2015**, *97*, 31–35. [CrossRef]

27. Reverchon, E.; Antonacci, A. Chitosan microparticles production by supercritical fluid processing. *Ind. Eng. Chem. Res.* **2006**, *45*, 5722–5728. [CrossRef]

28. Reverchon, E.; Spada, A. Erythromycin micro-particles produced by supercritical fluid atomization. *Powder Technol.* **2004**, *141*, 100–108. [CrossRef]

29. Wang, Q.; Guan, Y.-X.; Yao, S.-J.; Zhu, Z.-Q. Microparticle formation of sodium cellulose sulfate using supercritical fluid assisted atomization introduced by hydrodynamic cavitation mixer. *Chem. Eng. J.* **2010**, *159*, 220–229. [CrossRef]

30. Wu, H.-T.; Huang, S.-C.; Yang, C.-P.; Chien, L.-J. Precipitation parameters and the cytotoxicity of chitosan hydrochloride microparticles production by supercritical assisted atomization. *J. Supercrit. Fluids* **2015**, *102*, 123–132. [CrossRef]

31. Wu, H.-T.; Lee, H.-K.; Chen, H.-C.; Chien, L.-J. Precipitation kinetics and biological properties of chitosan microparticles produced using supercritical assisted atomization. *Chem. Eng. Res. Des.* **2015**, *104*, 615–625. [CrossRef]

32. Wu, H.-T.; Su, Y.-C.; Wang, Y.-M.; Tsai, H.-M. Characterisation and aerosolisation of mannitol particles produced using supercritical assisted atomization. *Chem. Eng. Res. Des.* **2018**, *137*, 308–318. [CrossRef]

33. Pielichowski, K.; Flejtuch, K.; Pielichowska, K. Differential scanning calorimetry studies on poly(ethylene glycol) with different molecular weights for thermal energy storage materials. *Polym. Adv. Technol.* **2002**, *13*, 690–696. [CrossRef]

34. Corrigan, D.O.; Healy, A.M.; Corrigan, O.I. The effect of spray drying solutions of polyethylene glycol (PEG) and lactose/PEG on their physicochemical properties. *Int. J. Pharm.* **2002**, *235*, 193–205. [CrossRef]

35. Ford, J.L.; Stewart, A.F.; Dubois, J.-L. The properties of solid dispersions of indomethacin or phenylbutazone in polyethylene glycol. *Int. J. Pharm.* **1986**, *28*, 11–22. [CrossRef]

36. Craig, D.Q.M.; Newton, J.M. Characterisation of polyethylene glycols using differential scanning calorimetry. *Int. J. Pharm.* **1991**, *74*, 33–41. [CrossRef]

Sample Availability: Samples of the compounds are not available from the authors.